DOI: 10.1002/chem.200600457

meso–meso-Linked Corrole Dimers with Modified Cores: Synthesis, Characterization, and Properties

Jeyaraman Sankar,[a] Harapriya Rath,[a] Viswanathan Prabhuraja,[a] Sabapathi Gokulnath,[a] Tavarekere K. Chandrashekar,*[a, b] Chandra Shekhar Purohit,[a] and Sandeep Verma*[a]

Abstract: The synthesis and characterization of the first examples of core-modified corrole dimers linked through the *meso* positions are described. The dimers are obtained by a simple Ag^{I}- or Fe^{III}-catalyzed coupling reaction in near-quantitative yields. The corroles obtained are metalated with metal ions, such as Cu^{II} and Ni^{II}. The electronic-absorption spectral studies reveal weak electronic interaction between the two subunits and the exciton coupling observed for the free-base corrole dimer (1717 cm^{-1}) is lower than that for the corresponding protonated derivative (4081 cm^{-1}). The solution-state structure derived from ^{1}H and two-dimensional NMR spectral studies reveals a noncoplanar arrangement of two corrole units. Geometry optimization at the B3LYP-631G level also confirms the noncoplanar arrangement of corroles with a dihedral angle of 64.8° between two corrole planes. The electron paramagnetic resonance (EPR) and magnetic characterization studies on the paramagnetic copper-metalated dimer indicate that both copper ions behave as independent spins without any noticeable interaction. Results of fluorescence studies reveal a bathochromic shift of about 60 nm upon dimerization. The first hyperpolarizability (β) measured by using the hyper Rayleigh scattering (HRS) method reveals doubling of the β values on progressing from monomer to dimer, attributed to enhanced π conjugation. The use of copper dimers in the photocleavage of DNA is also explored. It is shown that the bimetallic copper dimer selectively cleaves the nucleic acids without affecting the proteins, suggesting a possible application of the copper complex in the removal of nucleic acid contaminants from protein extracts through a simple photolytic pathway.

Keywords: core modification · corroles · DNA cleavage · nonlinear optics · porphyrinoids

Introduction

Synthetic porphyrin analogues are considered to be the ligands of choice to mimic natural processes, because of their similarity to natural systems in both structure and properties.[1] The recent availability of simpler synthetic methodologies allows their potential applications, such as optoelectronic materials, sensitizers in biomedical processes, and contrasting agents in magnetic resonance imaging (MRI), to be studied.[2] The main advantage of these macrocycles is their large delocalized π-electronic conjugation and their stability under the ambient conditions required for such applications. Hence, studies on extended conjugated macrocycles are of considerable interest. Such an extension in conjugation leads to a reduction in the HOMO–LUMO gap, thereby altering the energies of electronic transitions, shifting the absorption maxima to longer wavelengths.[3] Thus, these macrocycles can be used readily as biochemical sensitizers as their absorption maxima fall within the therapeutic window of 600–800 nm. A handful of methods to extend the basic π-delocalization pathway of porphyrins have been reported. One of these is to increase either the number of heterocyclic rings or the number of *meso* links that are connected to the pyrrolic rings, resulting in the formation of expanded porphyrins. The electronic and coordination chemistry of expanded porphyrins show interesting features and

[a] Dr. J. Sankar, Dr. H. Rath, V. Prabhuraja, S. Gokulnath, Prof. T. K. Chandrashekar, C. S. Purohit, Prof. S. Verma
Department of Chemistry, Indian Institute of Technology
Kanpur 208016 (India)
Fax: (+91) 512-259-7436
E-mail: tkc@iitk.ac.in
sverma@iitk.ac.in

[b] Prof. T. K. Chandrashekar
Present Address: Director, Regional Research Laboratory
Trivandrum, Kerala 695019 (India)

Supporting information for this article is available on the WWW under http://www.chemeurj.org/ or from the authors.

have been reviewed recently.[4] The alternative way to obtain the larger framework of π electrons is to connect individual porphyrin units to one another to make discrete oligomeric arrays of controllable length. In this context, Osuka and co-workers[5] synthesized a large multiporphyrin array **1** by linking the one *meso* position of the porphyrin with another porphyrin regioselectively through a silver-salt-mediated coupling methodology.

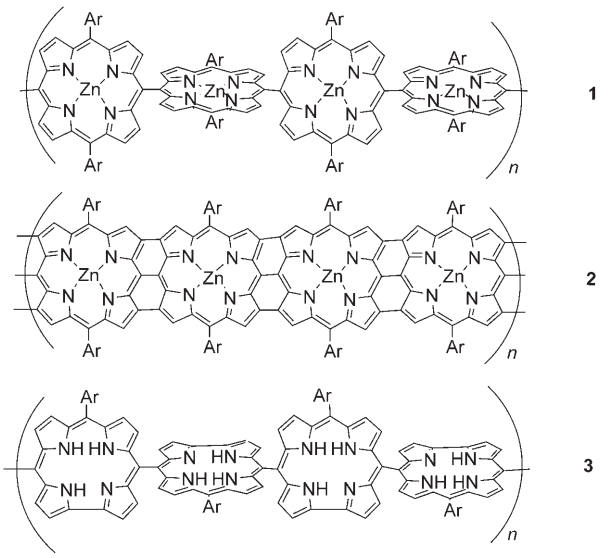

This results in the formation of covalently linked porphyrin oligomers with interesting physical and electronic properties. If the singly linked porphyrin arrays are further coupled with $Sc(OTf)_3$ and dichlorodicyanobenzoquinone (DDQ), *meso–meso*- and β–β doubly and triply linked porphyrin tapes **2** are formed.[6] The electronic interaction between each porphyrin unit makes it possible to alter the HOMO–LUMO gap to a considerable extent. These molecules are planar, as expected, and absorb in the near-infrared (NIR) region because of their hugely extended π delocalization. However, there are only a few reports of the use of the structurally similar 18π corroles as promising electronic materials. Corroles are also susceptible to forming multicorrole architectures, such as compound **3**, and here we report the synthesis of corrole dimers that are linked through *meso*-carbon centers.

Recent advances in corrole chemistry offer a variety of synthetic methods to obtain functionalized corroles in reasonable yields.[7] The problem of formation of porphyrin as a byproduct was successfully eliminated by optimizing the reaction conditions.[8] Reports from our laboratory have established the exclusive formation of core-modified corroles by three different [3+1] methodologies, providing the way for further studies.[9] The availability of such synthetic methods to obtain monomeric *meso*-free oxacorrole **4** as a single product in moderate yields prompted us to functionalize further the aforementioned corroles. The *meso*-free position of the monomeric oxacorrole is shown to be reactive under the *n*BuLi conditions to offer the *meso*-butylated corrole **5**.[10]

This provided the starting point to further modify the macrocycles to exploit their diverse properties. The *meso–meso*-linked corrole dimer is obtained by the direct coupling

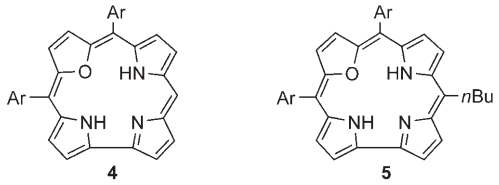

of the free-base corrole with AgOTf or $FeCl_3$ under ambient conditions in near-quantitative yields (90%). The resultant dimer is metalated with Ni^{II} and Cu^{II} and the electronic and electrochemical properties have been studied. These are the first examples in corrole chemistry to have a direct *meso–meso* link in contrast to a β–β-linked dicorrole, as reported by Gross and co-workers for the Co^{III}-metalation of the azatriphenyl corroles.[11] The electronic interaction between the individual corroles in the dicorrole moiety was probed by electronic-absorption and electrochemical studies. The nonlinear optics (NLO) properties of the corrole monomers and dimers were studied by the hyper Rayleigh scattering method (HRS) at 1064 nm. The moderate increase in the β values of the dimers relative to those of the monomers indicates the effect of extended π conjugation upon dimerization. The use of Cu^{II}-metalated dimer **9a** as a potential DNA-cleaving agent upon exposure to visible light is also highlighted.

Results and Discussion

The synthesis of *meso–meso*-linked porphyrin arrays was first established by Osuka and co-workers who used an efficient $AgPF_6$-mediated oxidative coupling strategy.[12] In this method, the Zn^{II} complex of 5,15-diaryl porphyrin having two substituent-free *meso* positions was reacted with silver hexafluorophosphate in the dark under nitrogen atmosphere to form the *meso–meso*-linked porphyrin oligomers. The reaction yielded the dimer as well as higher oligomers in comparable yields. The formation of these side products makes the separation process tedious. A mixture of oligomers was separated by repetitive HPLC-GPC and then purified by using silica-gel chromatography. The electronic and electrochemical properties of these porphyrin wires show moderate π conjugation between the rings, even though the neighboring porphyrin rings are expected to be nearly perpendicular to each other. The recent structural characterization confirms further the geometry of these novel macrocycles.[13]

To simplify the reaction by eliminating the formation of higher oligomers, monomeric *meso*-free oxacorrole **4** was employed to ensure the exclusive formation of **6**, thereby easing the purification process. If **4** was treated with $AgPF_6$

under the conditions reported by Osuka and co-workers,[12] the expected dimeric corrole could not be obtained. However, if the same reaction was repeated with AgOTf instead of $AgPF_6$, the dimer was isolated in about 90% yield (Scheme 1). This coupling of oxacorrole **4** with AgOTf was first noted in an attempt to metalate the macrocycle with the silver salt. A brown fraction was eluted from the basic alumina column after the metalation reaction. In the ^1H NMR spectrum of the pure fraction, the *meso*-CH signal was missing instead of the inner-pyrrole-NH signals. If the metalation had occurred, the NH signals should have been missing. But to our surprise, the NH signal was retained with a deshielded resonance. The β-hydrogen resonances were shifted slightly in the aromatic region (7–9 ppm) relative to those of **4**. The fast atom bombardment (FAB) mass spectra of the compound clearly revealed the composition of the dimers obtained (see Supporting Information). Prior to this, the same brown fraction was obtained during the metalation of **4** with $FeCl_3$ in dichloromethane. Even though the aryl–aryl coupling by $FeCl_3$ is a known method in polymerization reactions,[14] this is perhaps the first example to show that the same method can be used to couple larger aromatic systems, such as the 18π corroles described here. In both reactions, the dimer corrole **6** was the single product and neither the unreacted **4** nor the higher oligomers were obtained. If the same reaction was carried out by taking metalated monomers **7** and **8**, the reaction did not proceed in the expected way, but yielded inseparable mixtures. The coupling reaction is expected to proceed through a radical mechanism, and in our case the radical was observed immediately upon adding the free-base **4a** in dichloromethane to AgOTf in an electron paramagnetic resonance (EPR) tube (see Supporting Information).

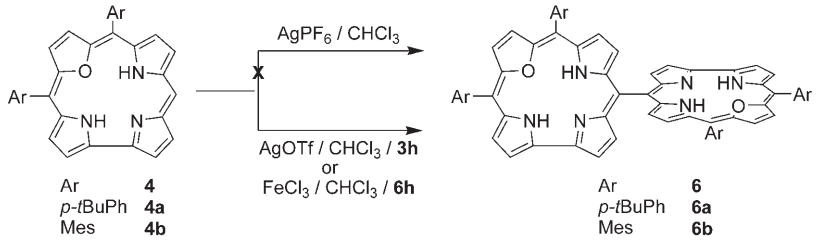

Scheme 1. Syntheses of the dimer corroles by the Ag^I- or Fe^{III}-catalyzed coupling reaction.

If the same reaction was monitored by performing EPR with $FeCl_3$, the radical signal could not be identified as a separate peak, probably because of the broad resonance of the catalyst itself. The free-base monomers and dimers were readily metalated in a single step by refluxing the $CHCl_3$/MeOH solvent mixture with the corresponding metal(II) acetates (Scheme 2). The Ni^{II} metalation was not successful with this solvent system and was achieved by refluxing the solution of the corrole in *N*,*N*-dimethylformamide (DMF) with the metal acetate in the presence of sodium acetate. The reactions were generally completed within 3 h. The mixture obtained was then evaporated under vacuum and separated by chromatography with neutral alumina to get the corresponding metal complexes. The heterometalation of the dimer corroles with a mixture of Ni^{II} and Cu^{II} acetates resulted in only dicopper-metalated derivatives, rather than the heterobimetallic dimer complexes. This can be attributed to the fact that the metalation of the dimer corroles with Cu^{II} acetate completes within 30 minutes and the Ni^{II}-metalation requires three hours. Therefore, it is the affinity of the corrole core for copper rather than nickel under ambient reaction conditions that facilitates the formation of a homobimetallic complex. Attempts to make heterobimetallic complexes, such as (Cu^{II}–Ni^{II}), were unsuccessful. We tried making monometallic dimers by controlling the amount of metal salts in the metalation reaction. Under these conditions, selective monometalation could not be achieved, probably because of the use of excess metal salts required for the metalation reactions. Selective demetalation by adding a controlled amount of acid resulted in demetalation of both the metal ions.

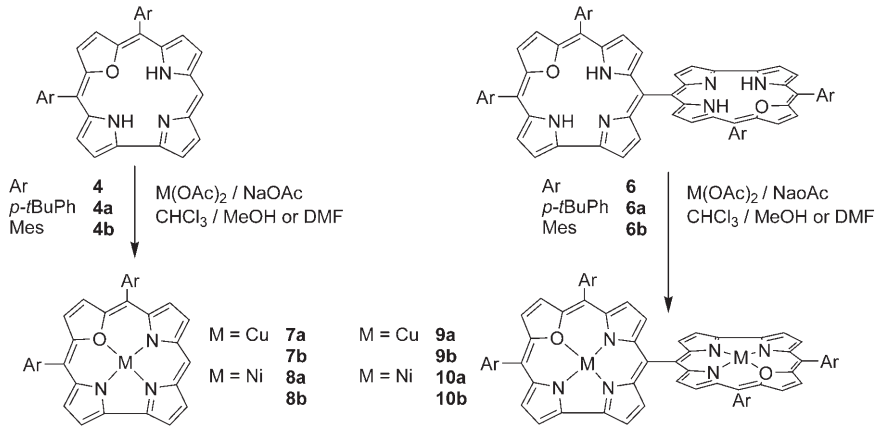

Scheme 2. Metalation of corroles.

Electronic-absorption spectra: The UV-visible spectrum of **6a** shows interesting features, with the intense Soret band at 417 nm followed by Q-type bands in the region 500–670 nm (Figure 1). The bathochromic shift of about 10 nm with respect to the monomer (Figure 2) is attributed to the increase in π delocalization after the coupling. The magnitude of the

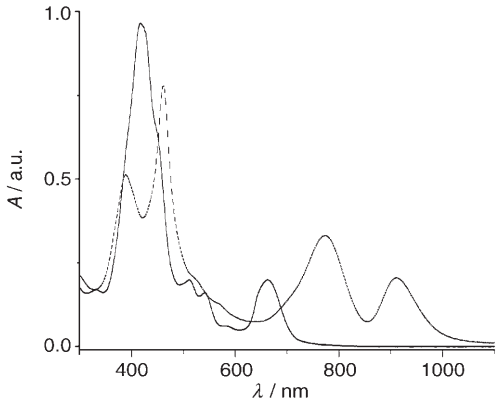

Figure 1. Electronic-absorption spectra of dimer corrole **6a** ($\sim 10^{-5}$ M) (——) and its protonated derivative **6a**·2H$^+$ (– – –) in CH_2Cl_2. The protonation was achieved by adding 10% v/v TFA in CH_2Cl_2.

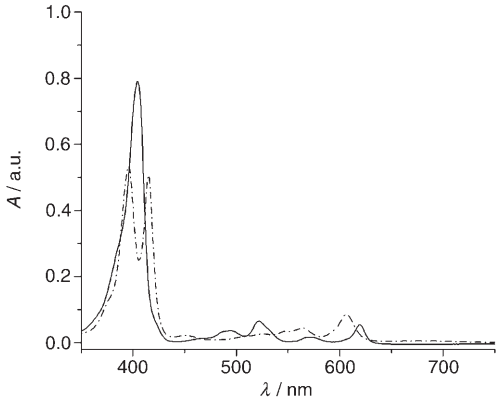

Figure 2. Electronic-absorption spectra of monomer corrole **4a** ($\sim 10^{-5}$ M) (——) and its protonated derivative **4a**·H$^+$ (–•–•–) in CH_2Cl_2. The protonation was achieved by adding 10% v/v TFA in CH_2Cl_2.

shift depends on the strength of electronic interaction between the two corrole moieties; large bathochromic shifts are observed for a stronger coupling.[3] The observation of a shift of only 10 nm in the present case suggests a weak interaction between the corrole moieties, which may be due to the absence of coplanarity between the two macrocycles. On the other hand, after protonation with trifluoroacetic acid (TFA), the Soret band is red-shifted to 461 nm with splitting. However, as reported previously,[10] the protonated form of the monomer deviates from planarity because of the expected steric congestion within the smaller corrole core and, therefore, the electronic spectrum tends to split. The exciton couplings calculated for the free-base (1717 cm^{-1}) and protonated (4081 cm^{-1}) corrole dimers clearly suggest a stronger interaction upon protonation. The same trend is observed in the case of **6b**, indicating that the corrole rings are intact with respect to the core structure, even after coupling. Another interesting feature in the protonated state is the appearance of a new Q-type band at around 911 nm. Taken together, all these features indicate the porphyrinic nature of the dimer **6a**. The UV-visible spectra of metal complexes of the macrocycles provide interesting patterns. The Ni^{II}-metalated **8a**,**b** and **10a**,**b** have three Soret-type peaks in the region of 390–410 nm and four Q-band-like absorptions in the region between 500 and 700 nm. The Cu^{II}-metalated **7a**,**b** and **9a**,**b** show a split Soret bands with nearly equal intensity.

^{1}H NMR characterization: The solution-state structure of **6a** was deduced from ^{1}H NMR and two-dimensional NMR experiments. The disappearance of the *meso*-CH signal at 9.6 ppm provides strong evidence that the coupling occurred at the free *meso* positions of oxacorrole **4a** to give **6a**. The resonance at −1.9 ppm was assigned to the inner-NH protons of the corrole core and the β-pyrrolic hydrogen resonances of the macrocycle have not shifted much relative to that of the monomer. The signal for the resonance of the inner-NH protons is deshielded with respect to monomer **4a** (~2.5 ppm). The single broad resonance obtained for the two different NH protons in the core is attributed to the plausible tautomerism expected for the corrole macrocycle. The spectrum recorded at 223 K gave only one broad signal, suggesting the presence of tautomerism even at 223 K. However, upon protonation of the macrocycle with TFA in $CDCl_3$ (10% v/v), three distinct NH signals were obtained at 253 K with δ values of −0.94, −2.29, and −3.83 ppm, consistent with our earlier observation for the core-modified corrole macrocycle. The values obtained here for **6a** are deshielded by nearly 1 ppm relative to that of the monomer **4a**.

Furthermore, the nickel-metalated dimer **10b** shows a well-resolved ^{1}H NMR spectrum in which the NH signals are missing and the β-pyrrolic proton resonances are well separated (Figure 3). The aromatic region of 8–10 ppm includes eight doublets accounting for the eight β-pyrrolic/furan protons. The protons of the mesityl ring resonate at around 7.23 ppm as a singlet, and at 7.16 and 7.13 ppm as two slightly separated singlets. The probable reason for the observation of these singlets may be that the mesityl protons are magnetically different. The assignments were made with the correlations obtained from two-dimensional COSY spectra (Figure 4). The resonances for the protons above and below the neighboring corrole ring (c′, d) resonate in the shielded region compared with the protons correlated to them (c, d′). This indicates that the individual corrole rings are nearly perpendicular to each other, as observed earlier in the case of porphyrins,[12] and the geometry around the Ni^{II} center is square-planar. The single-crystal X-ray structure of monomeric *meso*-phenyl Ni^{II} corrole **8** shows a perfect square-planar geometry around the Ni^{II} ion (see Supporting Information).

Structure optimization: Our efforts to obtain a single crystal suitable for X-ray analysis were not successful. Hence, optimization of the geometry by theoretical methods was carried out. The B3LYP-631G-level[22] optimized structure is shown in Figure 5. To simplify the analysis, *meso*-phenyl-substituted **6** was used and the substituents in the *meso*-phenyl groups were omitted. The optimized geometry pre-

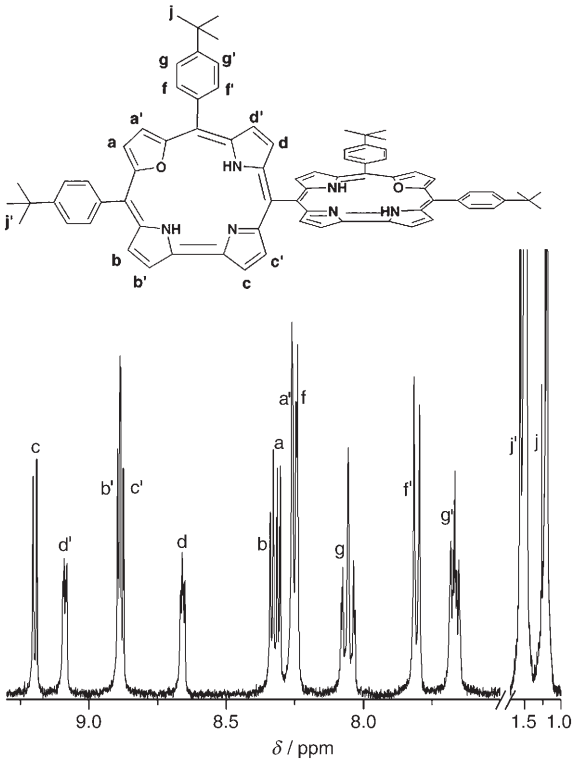

Figure 3. ^{1}H NMR spectrum and proton assignments for **6a** at RT in $CDCl_3$. The assignments are marked on the basis of correlations observed from $^{1}H\{^{1}H\}$ COSY experiments.

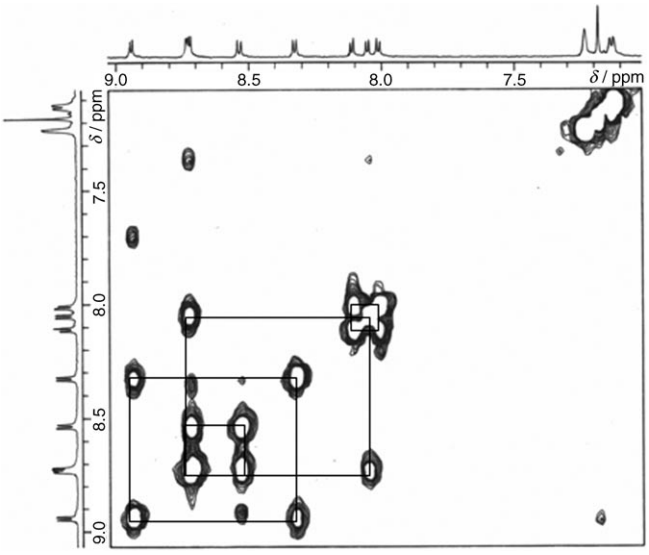

Figure 4. Two-dimensional COSY spectrum of **10b** recorded at 298 K in $CDCl_3$.

dicts that the two corrole moieties in **6** are not coplanar, as observed from spectroscopic methods, and are tilted with respect to each other at an angle of around 64.8°. The distance between the imaginary points at the centers of the corroles is about 8.45 Å. Furthermore, the phenyl rings attached to the macrocyclic core are also not in the plane of the respective corrole moieties and are tilted, although the angles of tilt are not the same for all the phenyl groups. The phenyl groups distal to the *meso–meso*-coupled vicinity are tilted at an average angle of ~55° and the phenyl groups proximal to the coupled vicinity are tilted at an average angle of ~70°. This may be attributed to the steric congestion created by the neighboring corrole ring in the former case. The assessments of the dihedral angles of phenyl groups and the angles between the planes of the corrole rings show that the electronic interactions between the corrole moieties do not depend on the structure of the individual rings, but rather on the conformation of the basic π-conjugation framework alone. This demonstrates an interesting point that the *meso–meso* linkage obtained has a marked influence on the electronic structure of the corrole macrocycle, similar to that observed for porphyrins.[13]

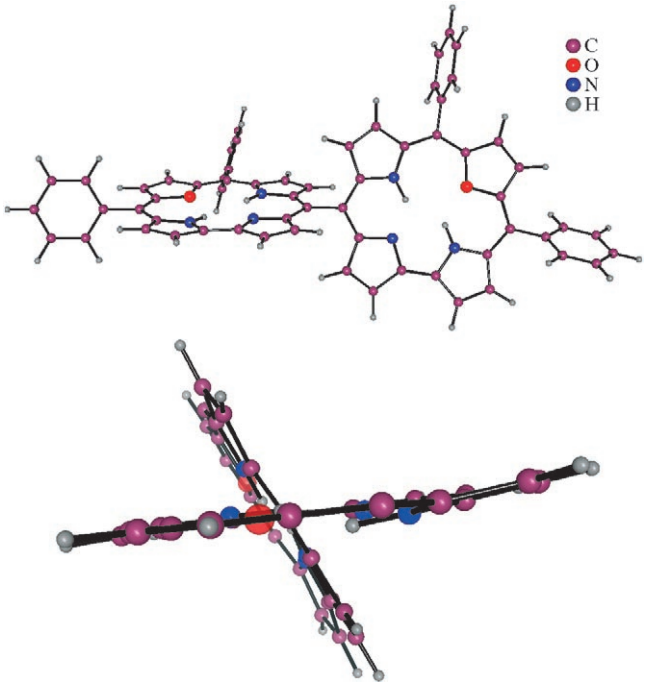

Figure 5. The B3LYP-631G-optimized structure of **6** (top) and its side view (bottom). Phenyl rings are omitted in the side view for clarity.

Electrochemical studies: The redox behavior of the reported compounds was studied by performing cyclic voltammetry with 0.1 M tetra-*n*-butylammonium hexafluorophosphate (TBAP) as supporting electrolyte in dichloromethane, in the potential range −1.8 to 1.8 V versus the saturated calomel electrode (SCE). A typical cyclic voltammogram scanned at a scan rate of 100 $mV s^{-1}$ for the representative examples is shown in Figure 6. The bifurcation of the first oxidation wave in the case of the dimer with respect to that of the monomer suggests plausible electronic interaction between the neighboring corrole rings. In the present case, the waves obtained within the positive-potential range do not have any well-defined reversible couple and, therefore, the peak value for the first oxidation wave was taken for the sake of

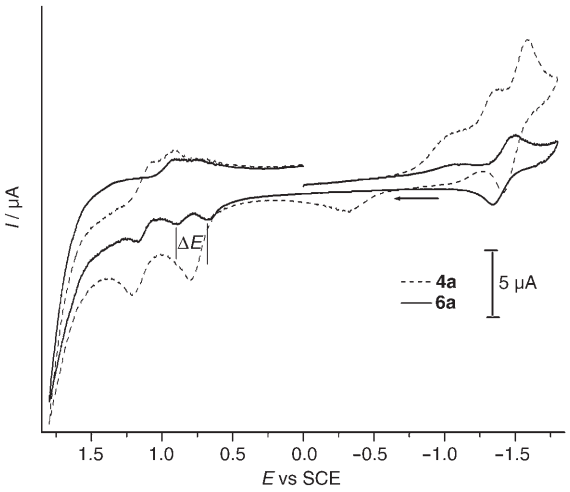

Figure 6. Cyclic voltammograms obtained for **4a** and **6a** with 0.1 M TBAP as the supporting electrolyte in CH_2Cl_2 and with SCE as the reference. The ΔE of **6a** is indicated.

comparison. The dimer **6a** (0.67 V) shows an easier oxidation than **4a** (0.79 V). The first oxidation wave observed for the monomer is split into two waves in the case of dimer. These waves are represented as E_{ox1} and E_{ox2} and the difference between them is denoted as ΔE in Table 1. The split-

Table 1. Redox potentials in CH_2Cl_2 with 0.1 M TBAP. Scan rate: 100 mV s^{-1}.

Compound	E_{ox1} [V]	E_{ox2} [V]	ΔE ($E_{ox1}-E_{ox2}$)
4a	0.79	–	–
6a	0.68	0.90	0.22
7a	0.72	–	–
9a	0.61	0.83	0.22
8a	0.83	–	–
10a	0.71	0.94	0.23

wave potentials are characteristic of the covalently linked porphyrin systems and represent the stepwise oxidation of each of the rings present in the dimer. The removal of one electron from the dimer makes the removal of one more electron from the skeleton more difficult and shifts the first oxidation potential of the other corrole moiety to a more-positive potential. This behavior is in good agreement with the electrochemical studies reported for the *meso–meso*-linked porphyrin dimers and directly linked N-confused porphyrin dimers.[15] This electronic interaction can be quantified by comparing the ΔE values. The ΔE values observed in the present case are slightly larger than those observed for porphyrin dimers. The difference in the redox behavior between the free-base and metalated species is small and indicates that the electronic interaction between the corrole rings is not altered to a notable extent after metalation, as expected for the porphyrin case. At this instant, no correlation between the electronegativity of the metal and redox properties could be evaluated. These higher values of ΔE for the macrocycles indicate that the corroles behave very differently after the first oxidation and the redox behavior of the macrocycle differs from related porphyrinic derivatives. The mesityl substitution in the *meso* position instead of *tert*-butylphenyl substitution does not show any marked effect on the redox properties.

Upon extending the π-delocalization pathway, that is, from monomer to dimer in free-base as well as in metalated cases, the oxidation becomes easier, suggesting a decrease in the HOMO–LUMO gap. The red shift of the absorption bands in dimers also justifies this conclusion. Furthermore, the difference between the first oxidation and first reduction potentials, which is a measure of the HOMO–LUMO gap, obtained for **6a** is around 2.09 V and for **4a** it is around 2.20 V. These redox properties suggest that the HOMO is becoming destabilized in the case of the dimers because of the expansion of the π-delocalization pathway, thereby reducing the HOMO–LUMO gap.

Fluorescence and lifetime studies: The emission properties of the macrocycles were probed in view of their different electronic structure. The emission maximum for **4a** was observed at 648 nm with a shoulder at 708 nm upon exciting at 419 nm. At exactly the same excitation wavelength, the dimer **6a** showed an emission at 711 nm with a red shift of almost 60 nm relative to that of the monomer. The fluorescence quantum yield of the dimer corrole (0.19) was nearly double that of the monomer (0.12) at 419 nm. The singlet lifetimes measured for **4a** ($\tau = 6.53$ ns (97.61)) and for **6a** ($\tau_1 = 1.8$ ns (50.61), $\tau_2 = 7.2$ ns (49.3)) did not show any marked change in progressing from monomer to dimer.

Nonlinear optical studies: Porphyrins are attractive targets for their application in nonlinear optics (NLO) because of their extended π delocalization. The relatively easy polarization of the π cloud facilitates an increase in the hyperpolarizability of the macrocycles, thereby making them the materials of choice. There are a handful of reports featuring various nonlinear-optical properties of porphyrins, such as first hyperpolarizability and two-photon absorption.[2] Our previous reports of the nonlinear properties of oxacorroles and oxasmaragdyrins proved that the extension of the π cloud enhances the nonlinear optical response recorded by using a *z*-scan technique.[16] Here, we used the hyper Rayleigh scattering (HRS) method to measure the first hyperpolarizability (β) of the corrole derivatives at 1064 nm in CH_2Cl_2 solutions. The first polarizabilities are dictated mainly by the nature and position of the donor and acceptor groups attached to the π system. At present, even though there are no functional groups, such as $-CN$, $-NO_2$, or $-NH_2$ placed at the periphery of the macrocycles to enhance the NLO response, the main aim is to correlate the influence of dimerization on the β values. It is well documented that the extended π-conjugation length contributes to a marked extent to the enhancement of β values. The values observed for the compounds **4a**–**10a** are given in Table 2. The highest value in the monomer series was observed for copper-metalated **7a** (17.7×10^{-30} esu) and in the dimer series for nickel-meta-

Table 2. First hyperpolarizability (β) values for various monomer- and dimer-corrole derivatives in CH_2Cl_2 by using the HRS technique.

Compound[a]	β_{HRS} [$\times 10^{-30}$ esu]	Compound[a]	β_{HRS} [$\times 10^{-30}$ esu]
4a	14.32	**9a**	31.7
6a	36.39	**8a**	13.48
7a	17.7	**10a**	43.09

[a] Only *tert*-butylphenyl-substituted derivatives are listed.

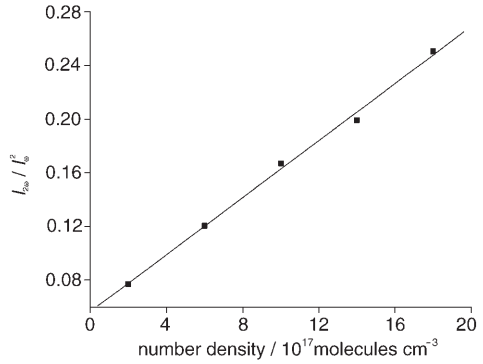

Figure 7. Dependence of the HRS intensity on the number density of **10a** at 1064 nm.

lated **10a** (43.1×10^{-30} esu). As a representative example, a plot of the dependence of the HRS intensity on the number density of the solute **10a** is given in Figure 7. From the slope of the plot, we extracted hyperpolarizability values relative to *p*-nitroaniline (*p*NA) as an external reference.

The open-shell (d^9) porphyrin complexes are reported[17] to have larger β values and in the present case we also observed the same trend. Although there was some increase in the β value for the Cu^{II}-metalated dimer, the large enhancement expected was not observed. Rather, the Ni^{II} dimer has the better response. This can be attributed to the fact that on dimerization, the electronic framework undergoes modification, thereby facilitating the nonlinear-response process in the case of **10a**. The general trend observed is that the values for the dimer series are nearly double those of the monomers. We conclude that the β values for the corroles are enhanced as the π-conjugation pathway progresses, as reported for porphyrins.[17c] A change in the *meso* substitution from **4a** to **4b** did not affect the nonlinear response to a great extent.

EPR and magnetic properties: To probe the interaction between the two paramagnetic metal centers in **9a**, EPR and magnetic measurements were recorded. The EPR spectra for compounds **7a** and **9a** were recorded in a CH_2Cl_2/toluene (1:1) solvent mixture and are shown in Figure 8. For the monomeric corrole **7a**, the EPR spectrum is very well resolved with the observation of both g and A parameters ($A_\parallel Cu = 182$ G, $A_\perp N = 15$ G, $A_\perp Cu = 30$ G, $g_\parallel = 2.23$, and $g_\perp = 2.03$). The pattern observed shows that the Cu^{II} ion is sitting inside the core with an almost square-planar geometry. However, in the case of **9a**, the room-temperature spectrum showed one broad resonance with $g = 2.05$ and a width of

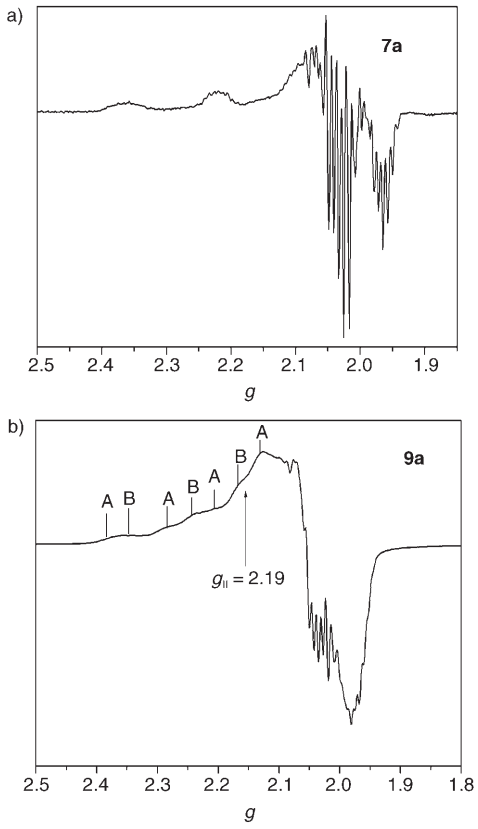

Figure 8. X-band EPR spectra recorded for a) **7a** and b) **9a** at 77 K in CH_2Cl_2/toluene (1:1). A and B correspond to two slightly different individual copper ions in dimer **9a**.

about 780 G. This spectrum was partly resolved as the temperature was reduced to 77 K.Furthermore, the super-hyperfine interactions were clearly visible. It can be understood that in the dimer case, the two copper(II) centers in the molecule are slightly different with respect to their environments, which causes their hyperfine splitting to overlap at low temperatures. The preservation of the EPR response even in the case of the dimer suggests that the two metal centers do not interact. The absence of a half-field resonance confirms that the two Cu^{II} nuclei are not interacting with each other. This is attributed to the large distance (~8.5 Å) between the cores of the individual corroles, as measured for the free-base dimer, which was further confirmed by results of magnetic studies carried out with the data obtained from superconducting quantum interference device (SQUID) measurements. The corrected μ_{eff} values for **7a** and **9a** are 1.54 and 1.60 BM, respectively, per copper center at 300 K (Figure 9).

DNA-cleavage studies: Porphyrins have been explored extensively for their applicability as sensitizers in photodynamic therapy (PDT).[18a] The structural and functional tunability of these macrocycles make them pharmaceutically attractive. There are several reports of the plasmid-relaxation properties of some water-soluble derivatives of tetrapyridyl porphyrin and ferric protoporphyrin IX.[18b] These natural and

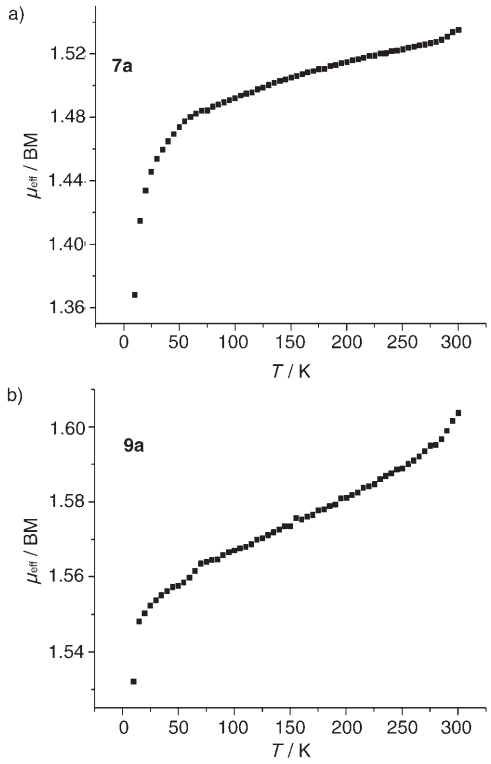

Figure 9. Dependence of μ_{eff} on temperature for a) **7a** and b) **9a**.

synthetic derivatives show remarkable DNA cleavage through either an oxidative or a photochemical pathway. In this context, we recently reported the utility of a hexacopper-metalated porphyrin-linked stannoxane cage showing selective DNA-cleavage activity, without the addition of any external cooxidant.[19]

These efforts led us to evaluate the viability of less-well-explored corrole macrocycles for their DNA-scission activity. The Cu^{II} complexes **7a** and **9a** were initially probed for the photocleavage of supercoiled DNA. Complete plasmid cleavage was noted for **9a** within four hours of irradiation with a tungsten lamp, suggesting possible generation of reactive species during photolysis (Figure 10, lanes 1–5). Interestingly, we were able to observe both the relaxed-circular and linear forms of the plasmid, which rapidly degraded to smaller fragments upon prolonged irradiation. However, in the case of **7a**, only the relaxed-circular DNA was formed without any further cleavage to linear DNA.

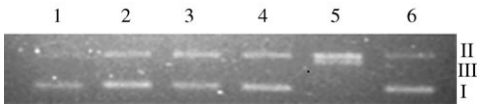

Figure 10. Photolytic plasmid relaxation by **9a**: lane 1, DNA alone; lanes 2–5, DNA+**9a** exposed to visible light (1, 2, 3, and 4 h, respectively); lane 6, DNA+**6a** irradiated for 4 h. (Form I: supercoiled DNA; form II: nickel circular DNA; form III: linear plasmid DNA.)

We decided to probe the nature of the reactive species formed during the reaction by performing chemical scavenger reactions that permit the detection of such species through their interaction with specific reagents. The photocleavage reaction was conducted in the presence of D-mannitol and *tert*-butanol to detect the formation of hydroxyl radicals during photolysis in aqueous buffer medium (Figure 11a, lanes 3 and 4, respectively). The reaction proceeded without any inhibition, suggesting that freely accessible, solvent-diffused free-radical species are probably not involved in the plasmid-relaxation process. However, appreciable quenching of the reaction was observed in the presence of NaN_3 (Figure 11a, lane 5). This suggests a close involvement of singlet-oxygen formation as a possible mechanism for DNA scission. This scenario was further confirmed by the inhibition of plasmid cleavage under anaerobic conditions. Complete inhibition of plasmid relaxation was observed if the reaction was performed under an oxygen-free nitrogen environment by using a freeze–thaw protocol (Figure 11b, lane 2), establishing a definitive role of oxygen in plasmid modification. As another control, we found that the free-base dimer **6a** was inactive, indicating the crucial role of coordinated copper(II) in plasmid relaxation by **9a**.

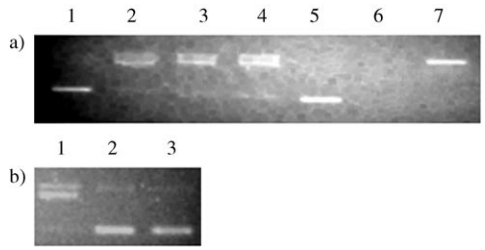

Figure 11. a) Scavanger gel: lane 1, DNA alone; lane 2, reaction for 4 h; lane 3, reaction in the presence of *tert*-butanol; lane 4, reaction in the presence of D-mannitol; lane 5, reaction in the presence of NaN_3; lane 6, reaction for 10 h; lane 7, reaction with **7a** for 4 h. b) Reaction under anaerobic conditions: lane 1, in air; lane 2, under nitrogen; lane 3, DNA alone.

Interestingly, this system proved ineffective towards protein modification, as probed by using lysozyme cleavage under tungsten-lamp irradiation (Figure 12). Detectable cleavage of the protein was not observed, indicating selectivity towards nucleic-acid cleavage, and even higher-molecular-weight cross-linked products were not apparent from gel electrophoresis analysis. The enhanced reactivity of the dimer corrole **9a** with respect to **7a** makes the covalently

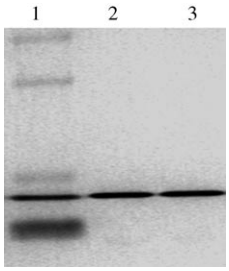

Figure 12. Lysozyme cleavage studied by using **9a**: lane 1, molecular weight markers (Da) 43000, 29000, 20100, 14300, 6500 (from top to bottom); lane 2, protein alone; lane 3, reaction mixture after 24 h of irradiation.

linked dimer attractive for these novel applications. Although the precise reasons are not yet clear, such discrimination should allow for specific photodegradation of nucleic acids in the cellular milieu by using PDT protocols.[20,21]

Conclusion

We have explored the successful synthesis of *meso–meso*-linked corrole dimers through a simple AgOTf- or $FeCl_3$-catalyzed oxidative-coupling reaction. This methodology is simple and gives near-quantitative yields. Spectroscopic and geometrical-optimization studies reveal that the two corrole rings are not planar and are oriented at a dihedral angle of 64.5° with respect to each other. This nonplanar geometry was retained upon metalation with Cu^{2+} and Ni^{2+}. A weak electronic interaction was observed between the two corrole subunits, as deduced from various spectroscopic and electrochemical studies. The possible application of these dimers as NLO materials and also as DNA-photocleavage agents was also explored. Further detailed studies are underway to explore this aspect of DNA cleavage.

Experimental Section

Electronic spectra were recorded by using a Perkin–Elmer Lambda 20 UV/Vis spectrophotometer. Proton NMR spectra in $CDCl_3$ were obtained by using a 400 MHz JEOL spectrometer and FAB-MS spectra were recorded by using a JEOL-SX-120/DA6000 spectrometer. Cyclic voltammetric studies were conducted by using an EG&G PARC model 273A. A three-electrode system consisting of a platinum working electrode, a platinum-mesh counter electrode, and a commercially available saturated calomel electrode (SCE) as the reference electrode was used.

General procedure for metalation of oxacorrole 4: For Ni^{II} and Cu^{II} metalation, the ligand was refluxed in $CHCl_3/CH_3OH$ or DMF containing the respective metal acetate in excess and sodium acetate for 2 h. The mixture was evaporated to dryness and then purified by chromatography on a neutral alumina column to obtain the pure metalated corroles.

Procedure for the dimerization reaction: The monomer corrole **4** was treated with 1 equiv of AgOTf or anhydrous $FeCl_3$ in chloroform and was stirred for 3 h in the dark under nitrogen atmosphere. The mixture was then evaporated and subjected to column chromatography over a silica-gel column to obtain a brown band. The fraction produced was purified further by using a basic alumina column to obtain pure dimer in about 90% yield. After performing the same reaction even in the presence of light and air, we noted no noticeable change in the yields of the dimer.

Compound **4** was treated with 1 equiv of anhydrous $FeCl_3$ for 6 h and the same procedure as for the AgOTf reaction was performed to obtain the pure dimer in about 85–90% yields.

Data for ***7a***: UV/Vis (CH_2Cl_2): $\lambda_{max}(\varepsilon)$=411 (9.8), 424 (9.6), 546 (1.4), 566 (1.3), 609 nm (1.4×10^{-4} M^{-1}cm^{-1}); FAB-MS: *m/z* (%): 624 (100); elemental analysis calcd (%) for $C_{39}H_{35}CuN_3O$: C 74.92, H 5.64, N 6.72; found: C 74.94, H 5.63, N 6.70.

Data for ***7b***: UV/Vis (CH_2Cl_2): $\lambda_{max}(\varepsilon)$=410 (9.7), 424 (9.7), 544 (1.4), 568 (1.3), 609 nm (1.2×10^{-4} M^{-1}cm^{-1}); FAB-MS: *m/z* (%): 596 (100); elemental analysis calcd (%) for $C_{37}H_{31}CuN_3O$: C 74.41, H 5.23, N 7.04; found: C 74.44, H 5.21, N 7.03.

Data for ***8a***: ^{1}H NMR (400 MHz, $CDCl_3$, 25°C, TMS): δ=9.46 (s, 1H), 9.02 (d, *J*=4.4 Hz, 1H), 8.92 (d, *J*=6 Hz, 1H), 8.91 (d, *J*=4.4 Hz, 1H), 8.86 (d, *J*=4.8 Hz, 1H), 8.8 (d, *J*=3.2 Hz, 1H), 8.75 (d, *J*=6 Hz, 1H), 8.46 (d, *J*=4.8 Hz, 1H), 8.41 (d, *J*=3.6 Hz, 1H), 7.97 (d, *J*=8 Hz, 2H), 7.88 (d, *J*=6.8 Hz, 2H), 7.48 (m, 4H), 1.55 (s, 9H), 1.52 ppm (s, 9H); UV/Vis (CH_2Cl_2) $\lambda_{max}(\varepsilon)$=325 (1.6), 371 (4.9), 394 (7.8), 413 (6.1), 431 (5.7), 553 (1.1), 575 (1.3), 597 nm (0.1×10^{-4} M^{-1}cm^{-1}); FAB-MS: *m/z* (%): 619 (100); elemental analysis calcd (%) for $C_{39}H_{35}N_3NiO$: C 75.50, H 5.69, N 6.77; found: C 75.52, H 5.68, N 6.75.

Data for ***8b***: ^{1}H NMR (400 MHz, $CDCl_3$, 25°C, TMS): δ=9.48 (s, 1H), 9.02 (d, *J*=4.4 Hz, 1H), 8.91 (d, *J*=6 Hz, 1H), 8.9 (d, *J*=4.4 Hz, 1H), 8.88 (d, *J*=4.4 Hz, 1H), 8.8 (d, *J*=3.2 Hz, 1H), 8.72 (d, *J*=6 Hz, 1H), 8.44 (d, *J*=4.8 Hz, 1H), 8.41 (d, *J*=3.2 Hz, 1H), 7.19 (s, 4H), 2.54 (s, 3H), 2.52 (s, 3H), 1.8 (s, 6H), 1.74 ppm (s, 6H); UV/Vis (CH_2Cl_2): $\lambda_{max}(\varepsilon)$=324 (1.6), 371 (5.0), 393 (7.7), 414 (6.0), 433 (5.7), 551 (1.1), 572 (1.2), 596 nm (0.1×10^{-4} M^{-1}cm^{-1}); FAB-MS: *m/z* (%): 591 (100); elemental analysis calcd (%) for $C_{37}H_{31}N_3NiO$: C 75.02, H 5.27, N 7.09; found: C 75.05, H 5.25, N 7.08.

Data for ***6a***: ^{1}H NMR (400 MHz, $CDCl_3$, 25°C, TMS): δ=9.19 (d, *J*=5 Hz, 2H), 9.07 (br, 2H), 8.87 (m, 4H), 8.65 (br, 2H), 8.33 (d, *J*=4.6 Hz, 2H), 8.31 (d, *J*=4.2 Hz, 2H), 8.24 (m, 6H), 8.04 (m, 4H), 7.79 (d, *J*=8 Hz, 4H), 7.65 (m, 4H), 1.54 (s, 18H), 1.5 (s, 18H), −1.9 ppm (br s, 4NH); UV/Vis (CH_2Cl_2): $\lambda_{max}(\varepsilon)$=417 (8.7), 511 (1.8), 541 (1.5), 585 (0.5), 662 nm (1.8×10^{-4} M^{-1}cm^{-1}); FAB-MS: *m/z* (%): 1126 (100); elemental analysis calcd (%) for $C_{78}H_{72}N_6O_2$: C 83.24, H 6.45, N 7.47; found: C 83.27, H 6.41, N 7.42.

Data for ***6b***: ^{1}H NMR (400 MHz, $CDCl_3$, 25°C, TMS): δ=9.04 (br, 2H), 8.88 (d, *J*=3.6 Hz, 2H), 8.73 (d, *J*=4.4 Hz, 2H), 8.62 (d, *J*=4 Hz, 2H), 8.4 (s, 2H), 8.3 (m, 4H), 8.1 (d, *J*=4 Hz, 2H), 7.26 (s, 8H), 1.91 (s, 12H), 1.86 (s, 12H), 1.82 (s, 12H), −1.91 ppm (br s, 4NH); UV/Vis (CH_2Cl_2): $\lambda_{max}(\varepsilon)$=416 (8.8), 511 (1.6), 540 (1.5), 583 (0.6), 661 nm (1.8×10^{-4} M^{-1}cm^{-1}); FAB-MS: *m/z* (%): 1069 (100); elemental analysis calcd (%) for $C_{74}H_{64}N_6O_2$: C 83.12, H 6.03, N 7.86; found: C 83.16, H 5.96, N 7.82.

Data for ***9a***: UV/Vis (CH_2Cl_2): $\lambda_{max}(\varepsilon)$=429 (15.9), 443 (16.7), 523 (2.4), 564 (2.6), 642 nm (3.6×10^{-4} M^{-1}cm^{-1}); FAB-MS: *m/z* (%): 1247 (100); elemental analysis calcd (%) for $C_{78}H_{68}Cu_2N_6O_2$: C 75.04, H 5.49, N 6.73; found: C 75.06, H 5.47, N 6.71.

Data for ***9b***: UV/Vis (CH_2Cl_2): $\lambda_{max}(\varepsilon)$= 428 (15.7), 443 (16.5), 525 (2.3), 566 (2.5), 643 nm (3.7×10^{-4} M^{-1}cm^{-1}); FAB-MS: *m/z* (%): 1190 (100); elemental analysis calcd (%) for $C_{74}H_{60}Cu_2N_6O_2$: C 74.50, H 5.07, N 7.05; found: C 74.51, H 5.04, N 7.02.

Data for ***10a***: ^{1}H NMR (400 MHz, $CDCl_3$, 25°C, TMS): δ=9.14(d, *J*=5.2 Hz, 2H), 9.01 (d, *J*=4.4 Hz, 2H), 8.83 (d, *J*=5.2 Hz, 2H), 8.75 (d, *J*=4.4 Hz, 2H), 8.58 (d, *J*=4 Hz, 2H), 8.22 (d, *J*=4.8 Hz, 2H), 8.17 (d, *J*=4.4 Hz, 2H), 8.13 (m, 4H), 8.07 (d, *J*=4.4 Hz, 2H), 7.98 (m, 4H), 7.76 (d, *J*=8 Hz, 4H), 7.63 (d, *J*=6.8 Hz, 4H), 1.55 (s, 18H), 1.45 ppm (s, 18H); UV/Vis (CH_2Cl_2): $\lambda_{max}(\varepsilon)$=329 (2.3), 374 (6.5), 399 (8.0), 434 (7.5), 456 (10.5), 564 (1.8), 593 (1.9), 626 nm (2.8×10^{-4} M^{-1}cm^{-1}); FAB-MS: *m/z* (%): 1236 (100); elemental analysis calcd (%) for $C_{78}H_{68}N_6Ni_2O_2$: C 75.62, H 5.53, N 6.78; found: C 75.64, H 5.51, N 6.76.

Data for ***10b***: ^{1}H NMR (400 MHz, $CDCl_3$, 25°C, TMS): δ=8.94 (d, *J*=4 Hz, 2H), 8.73 (m, 4H), 8.53 (d, *J*=5.4 Hz, 2H), 8.33 (d, *J*=4.4 Hz, 2H), 8.11 (d, *J*=4.6 Hz, 2H), 8.05 (d, *J*=4.4 Hz, 2H), 8.01 (d, *J*=4.8 Hz, 2H), 7.23 (s, 4H), 7.14 (s, 2H), 7.13 (s, 2H), 2.55 (s, 6H), 2.45 (s, 6H), 1.87 (s, 6H), 1.85 (s, 6H), 1.81 (s, 6H), 1.78 ppm (s, 6H); UV/Vis (CH_2Cl_2): $\lambda_{max}(\varepsilon)$=328 (2.2), 375 (6.6), 401 (7.8), 433 (7.4), 458 (10.5), 566 (1.9), 594 (1.9), 628 nm (2.7×10^{-4} M^{-1}cm^{-1}); FAB-MS: *m/z* (%): 1180 (100); elemental analysis calcd (%) for $C_{74}H_{60}N_6Ni_2O_2$: C 75.15, H 5.11, N 7.11; found: C 75.17, H 5.07, N 7.09.

Acknowledgements

We thank DST, New Delhi, for financial support. J.S., H.R., V.P.R., S.G., and C.S.P. thank CSIR, New Delhi, for fellowships. We thank Prof. P. K. Das, IISc, Bangalore, for the HRS measurements and Dr. M. M. Balamurali for his help in theoretical structure optimization.

[1] J. L. Sessler, S. J. Weghorn in *Expanded, Contracted, and Isomeric Porphyrins, Tetrahedron Organic Chemistry Series, Vol. 15*, Pergamon, New York, **1997**, pp. 11–125.
[2] a) R. Paolesse in *Porphyrin Handbook, Vol. 2* (Eds.: K. M. Kadish, K. M. Smith, R. Guilard), Academic Press, San Diego, CA, **2000**, pp. 201–232; b) J.-H. Chou, M. E. Kosal, H. S. Nalwa, N. A. Rakow, K. S. Suslick in *Porphyrin Handbook, Vol. 6* (Eds.: K. M. Kadish, K. M. Smith, R. Guilard), Academic Press, San Diego, CA, **2000**, pp. 43–131.
[3] D. Kim, A. Osuka, *Acc. Chem. Res.* **2004**, *37*, 735–745.
[4] T. K. Chandrashekar, S. Venkatraman, *Acc. Chem. Res.* **2004**, *36*, 676–691.
[5] A. Osuka, H. Shimidzu, *Angew. Chem.* **1997**, *109*, 93–95; *Angew. Chem. Int. Ed. Engl.* **1997**, *36*, 135–137.
[6] A. Tsuda, A. Osuka, *Science* **2001**, *293*, 79–82.
[7] D. T. Gryko, *Eur. J. Org. Chem.* **2002**, 1735–1743.
[8] Z. Gross, N. Galili, I. Saltsman, *Angew. Chem.* **1999**, *111*, 1530–1533; *Angew. Chem. Int. Ed.* **1999**, *38*, 1427–1429.
[9] J. Sankar, H. Rath, V. Prabhuraja, T. K. Chandrashekar, J. J. Vittal, *J. Org. Chem.* **2004**, *69*, 5135–5138.
[10] J. Sankar, V. G. Anand, S. Venkatraman, H. Rath, T. K. Chandrashekar, *Org. Lett.* **2002**, *4*, 4233–4235.
[11] A. Mahammed, I. Giladi, I. Goldberg, Z. Gross, *Chem. Eur. J.* **2001**, *7*, 4259–4265.
[12] A. Tsuda, A. Nakano, H. Furuta, H. Yamochi, A. Osuka, *Angew. Chem.* **2000**, *112*, 572–575; *Angew. Chem. Int. Ed.* **2000**, *39*, 558–561.
[13] N. Aratani, A. Takagi, Y. Yanagawa, T. Matsumoto, T. Kawai, Z. S. Yoon, D. Kim, A. Osuka, *Chem. Eur. J.* **2005**, *11*, 3389–3404.
[14] M. Svensson, M. Theander, O. Ingänos, M. R. Andersson, *Synth. Met.* **2001**, *119*, 113–114.
[15] a) A. Tsuda, H. Furuta, A. Osuka, *J. Am. Chem. Soc.* **2001**, *123*, 10304—10321; b) P. J. Chmielewski, *Angew. Chem.* **2004**, *116*, 5773–5776; *Angew. Chem. Int. Ed.* **2004**, *43*, 5655–5658.
[16] S. Venkatraman, R. Kumar, J. Sankar, T. K. Chandrashekar, K. Sendhil, C. Vijayan, A. Kelling, M. O. Senge, *Chem. Eur. J.* **2004**, *10*, 1423–1432.
[17] a) A. Sen, P. C. Ray, P. K. Das, V. Krishnan, *J. Phys. Chem.* **1996**, *100*, 19611–19613; b) A. Sen, V. Krishnan, *J. Chem. Soc. Faraday Trans.* **1997**, *93*, 4281–4288; c) D. Y. Kim, T. K. Ahn, J. H. Kwon, D. Kim, T. Ikeue, N. Aratani, A. Osuka, M. Shigeiwa, S. Maeda, *J. Phys. Chem. A* **2005**, *109*, 2996–2999.
[18] a) G. Pratviel, J. Bernadou, B. Meunier, *Adv. Inorg. Chem.* **1998**, *45*, 251–312; b) B. Meunier, A. Robert, G. Pratviel, J. Bernadou in *Porphyrin Handbook, Vol. 4* (Eds.: K. M. Kadish, K. M. Smith, R. Guilard), Academic Press, San Diego, CA, **2000**, pp. 119–188.
[19] V. Chandrasekhar, S. Nagendran, R. Azhakar, K. R. Kumar, A. Srinivasan, K. Ray, T. K. Chandrashekar, C. Madhavaiah, S. Verma, U. D. Priyakumar, G. N. Sastry, *J. Am. Chem. Soc.* **2005**, *127*, 2410–2411.
[20] S. Dhar, D. Senapati, P. K. Das, P. Chattopadhyay, M. Nethaji, A. R. Chakravarty, *J. Am. Chem. Soc.* **2003**, *125*, 12118–12124.
[21] L. Gude, M.-J. Fernández, K. B. Grant, A. Lorente, *Org. Biomol. Chem.* **2005**, *3*, 1856–1862.
[22] Gaussian 98 (Revision A.9), M. J. Frisch, G. W. Trucks, H. B. Schlegel, G. E. Scuseria, M. A. Robb, J. R. Cheeseman, V. G. Zakrzewski, J. A. Montgomery, Jr., R. E. Stratmann, J. C. Burant, S. Dapprich, J. M. Millam, A. D. Daniels, K. N. Kudin, M. C. Strain, O. Farkas, J. Tomasi, V. Barone, M. Cossi, R. Cammi, B. Mennucci, C. Pomelli, C. Adamo, S. Clifford, J. Ochterski, G. A. Petersson, P. Y. Ayala, Q. Cui, K. Morokuma, D. K. Malick, A. D. Rabuck, K. Raghavachari, J. B. Foresman, J. Cioslowski, J. V. Ortiz, A. G. Baboul, B. B. Stefanov, G. Liu, A. Liashenko, P. Piskorz, I. Komaromi, R. Gomperts, R. L. Martin, D. J. Fox, T. Keith, M. A. Al-Laham, C. Y. Peng, A. Nanayakkara, C. Gonzalez, M. Challacombe, P. M. W. Gill, B. G. Johnson, W. Chen, M. W. Wong, J. L. Andres, M. Head-Gordon, E. S. Replogle, J. A. Pople, Gaussian, Inc., Pittsburgh, PA, **1998**.

Received: April 3, 2006
Published online: September 22, 2006

